Journal of Applied Sciences

ISSN 1812-5654

science alert

ANSInet
an open access publisher
http://ansinet.com

Journal of Applied Sciences 11 (16): 2932-2939, 2011
ISSN 1812-5654 / DOI: 10.3923/jas.2011.2932.2939

Simulation of n_1-p_2 Microcrystalline Silicon Tunnel Junction with AMPS-1D in a-Si :H/μc-Si :H Tandem Solar Cells

Abbas Belfar and Rachida Mostefaoui
Laboratory of Plasma Physics, Conductor Materials and their Applications,
University of Sciences and Technology M.B. Oran, El-m'naouer POB.1505, Oran 31000, Algeria

Abstract: The electrical properties of a-Si:H/μc-Si:H micromorph tandem solar cells was studied with computer simulation. In this study, AMPS (Analysis of microelectronic and photonic structure)-1D is used to study the output parameters, Short circuit current (J_{sc}), open-circuit Voltage (V_{oc}), Fill Factor (FF) and Efficiency (η) of single (a-Si:H, μc-Si:H) and (a-Si:H/μc-Si:H) double junction solar cells. The carrier transport at the junction between the two p-i-n subcells is simulated with the help of a thin heavily defective Recombination Layer (RL) with a reduced mobility gap. The comparison between the output parameters of the above different types solar cells is given. The substitution of the N_1 (a-Si:H) layer by a N_1 (μc-Si:H) layer in the tandem structure (P_1-I_1-N_1/RL/P_2-I_2-N_2) leads to an improvement of the output cell parameters : J_{sc} increases from 11.607 to 12.00 mA cm^{-2}, FF increases from 0.670 to 0.710, the V_{oc} increases from 1.347 V to 1.541 V and the efficiency increases from 10.460 to 13.127%. Moreover, the impact of the N_1 layer and the profiling in the energy band gap realized by N_1-P_2 microcrystalline tunnel junction at the characteristics of tandem solar cells is also studied in this study.

Key words: Micromorph, microcrystalline silicon, tandem solar cells, tunnel junction, AMPS-1D

INTRODUCTION

Micromorph tandem solar cells consisting of an amorphous silicon top cell and a microcrystalline bottom cell is one of the most promising new thin-film silicon solar-cell concepts. Their promise lies in the hope of simultaneously achieving high conversion efficiencies at relatively low manufacturing costs. The key element of the micromorph cell is the hydrogenated microcrystalline silicon bottom cell that opens new perspectives for low-temperature thin-film crystalline silicon technology. So far, stabilized efficiencies of about 12% (10.7% independently confirmed) could be obtained with micromorph solar cells (Keppner *et al*., 1999; Khosroshahi *et al*., 2008). Hydrogenated microcrystalline silicon (μc-Si:H) was originally introduced by Veprek and Marecek (1968), Veprek and Veprek-Heijman (1991) and Ahmed *et al*. (2008) and is nowadays generally obtained by a Plasma Enhanced Chemical Vapour Deposition (PECVD) process using a mixture of silane and hydrogen. Due to its efficient doping properties, both for n-type as well as p-type material, μc-Si:H was form the beginning successfully used as ohmic contact layers in solar cells and in thin-film transistors (Keppner *et al*., 1999; Khatib *et al*., 2009; Hamel and Chibani, 2010). To use microcrystalline silicon alone as an active absorber layer in solar cells was, due to the reasons mentioned above, for many years not seriously taken into account for solar cell applications. The IMT Neuchâtel also used a polymer substrate foil and obtained a stabilized solar energy conversion efficiency of 7% for a single junction a-Si:H solar cell and 8.3% for a small-area tandem junction a-Si:H/μc-Si:H solar cell (Van den Donkera *et al*., 2007; Al-Hadidi and Ibrahim, 2008).

SIMULATION MODEL

AMPS can simulate an extremely general semiconductor device structure. In the present version of AMPS-1D there are two different approaches (1) Density of States (DOS) picture and (2) carrier lifetime picture. The DOS picture is well suited for materials like a-Si:H and μc-Si:H thin films due to the large defect densities in Grain Boundaries (Gbs) (Tripathi and Dusane, 2006).

In the electrical part of the model, three coupled differential equations: the Poisson's equation and the two carrier continuity equation are solved simultaneously under non-equilibrium steady state conditions (i.e., under the effect of voltage or light bias, or both) by using the method of finite differences and Newton-Raphson technique, directly from the first principles. The equations used are:

Corresponding Author: Abbas Belfar, Laboratory of Plasma Physics, Conductor Materials and their Applications, University of Sciences and Technology M.B. Oran, El-m'naouer POB.1505, Oran 31000, Algeria

Poisson's equation:

$$\frac{\partial^2 \psi(x)}{\partial^2 x} = \frac{\rho(x)}{\varepsilon} \quad (1)$$

Hole continuity equation:

$$G(x) - R(p(x), n(x)) - \frac{1}{q}\frac{\partial J_p(x)}{\partial x} = 0 \quad (2)$$

Electron continuity equation:

$$G(x) - R(p(x), n(x)) + \frac{1}{q}\frac{\partial J_n(x)}{\partial x} = 0 \quad (3)$$

where $\rho(x)$ is the net charge density.

$$\rho(x) = q\left[p(x) - n(x) + p_T(x) - n_T(x) + N^+_{net}\right] \quad (4)$$

and the electric field:

$$E = \frac{\partial \Psi(x)}{\partial x} \quad (5)$$

where, ε is the dielectric constant, E the electrostatic field, $\Psi(x)$ represents the position in energy of the local vacuum level, x the position in the device, p and n the valence-band hole density and the conduction band electron density, respectively, q the electronic charge, R the recombination rate, p_T and n_T the trapped hole and electron population density, respectively, N^+_{net} the net doping density, if any, G the electron-hole pair generation rate, J_p and J_n the hole and electron current density respectively and E_{Fp} and E_{Fn} the hole and electron quasi-Fermi levels. In our calculations, the three state variables that completely define the state of a device have been taken to be the local vacuum level, Ψ and the quasi-Fermi levels E_{Fp} and E_{Fn}. Once these three dependent variables are known as a function of x, all other information about the system can be determined as functions of position. In thermodynamic equilibrium, the Fermi level is a constant as a function of position and hence the three Eq. (1-3) essentially reduce to only one equation viz., the Poisson's equation. Therefore, the local vacuum level $\Psi(x)$ is the only unknown to be solved for in thermodynamic equilibrium.

In the non-thermodynamic equilibrium steady-state, a system of three coupled non-linear second order differential equations in the three unknowns (Ψ, E_{Fn}, E_{Fp}) are obtained. In order to solve these equations for our state variables (Ψ, E_{Fn}, E_{Fp}), we need six boundary conditions, two for each dependent variable. The first two boundary conditions are modified versions of the ones used for solving Poisson's equation in thermodynamic equilibrium:

$$\psi(0) = 0 - \chi(L) - \varphi_{bL} + \varphi_{bo} + \chi(0) - V \quad (6)$$

and

$$\psi(L) = 0 \quad (7)$$

where, L is the length of the device, $\chi(0)$, $\chi(L)$ are the electron affinities at x = 0 and x = L, respectively and V is the applied voltage. It should also be mentioned here that the zero of $\Psi = \Psi(x)$ is chosen to be the position in energy of the vacuum level at the boundary point x = L. The two boundary conditions for the Poisson's equation in thermodynamic equilibrium are Eq. 6 with the applied voltage V term absent and Eq. 7. The four other boundary conditions are obtained from imposing constraints on the currents at the boundaries at x = 0 and x = L. These constraints force the mathematics to acknowledge the fact that the currents must cross at x = 0 and x = L (the contact positions) by either thermionic emission or interface recombination. Expressed mathematically, we obtain the following:

$$J_n(0) = qS_{n0}\left[n(0) - n_0(0)\right] \quad (8)$$

$$J_p(0) = qS_{p0}\left[p(0) - p_0(0)\right] \quad (9)$$

$$J_n(L) = qS_{nL}\left[n(L) - n_0(L)\right] \quad (10)$$

$$J_p(L) = qS_{pL}\left[p(L) - p_0(L)\right] \quad (11)$$

where, S_{no}, S_{po} are surface recombination velocities for electrons and holes respectively at the x = 0 interface and the quantities S_{nL}, S_{pL} are the corresponding velocities at the x = L interface. The largest value they can have is $\sim 10^7$ cm sec^{-1} dictated by thermionic emission. Here, n (0) (p (0))are the electron (hole) density at x = 0, n (L) (p (L)) are the same at x = L.

n_o (0) (p_0 (0)), n_0 (L) (p_0 (L)) are the electron (hole) density in the thermodynamic equilibrium at x = 0 and x = L, respectively. With the help of the boundary conditions stated above, the three Eq. 1 to 3 can be solved simultaneously for $\Psi = \Psi(x)$, $E_{fn} = E_{fp}(x)$ and $E_{Fp} = E_{Fp}(x)$. For this, the different terms in the equations are to be calculated first. The gap state model used in our calculations consists of the tail states and two Gaussian distribution functions to simulate the deep dangling bond states. The generation term in the continuity equations

has been calculated using a semiempirical model (Leblanc *et al*., 1994) that has been integrated into the modelling program. Both specular interference effects and diffused reflectances and transmittances due to interface roughness are taken into account.

MICROMORPH SOLAR CELLS

General aspects: The combination of an amorphous silicon top cell with a microcrystalline silicon bottom cell to form a stacked tandem cell is called the micromorph cell.

The different gap energies involved in the micromorph tandem cell of the top and of the bottom cell make a striking difference to the well-known double-junction a-Si:H/a-Si:H tandem cell. The concept of superposing two a-Si:H cells is based on the reduction in the Staebler-Wronski (Staebler and Wronski, 1977) effect that can be obtained by keeping each individual i-layer as thin as possible and not on a better utilization of the solar spectrum.

Whereas the double-junction concept for a-Si:H cells is useful for reducing light-induced degradation, that the micromorph tandem cells offers further the possibility of a better utilisation of the sun spectrum. A possibility that is also realized with a-Si:H/a-SiGe:H stacked cells, yet to a larger extent, as it is so far not possible to obtain low enough band gaps with device-quality amorphous silicon-germanium alloys (Keppner *et al*., 1999).

Stability: The stable μc-Si:H bottom cell contributes to a better stability of the entire micromorph tandem cell under light-soaking. It could, in fact, be shown that the light-induced degradation of the micromorph cell is due to the amorphous top cell alone (Shah *et al*., 2000). In a First attempt to a further increase in stable efficiency, one can use a thicker bottom cell that could deliver an enhanced photocurrent without running itself into stability problems. The concept of a micromorph solar cell brings progress via a new stable bottom cell into the thin-films silicon scenario, the stability of the amorphous silicon top cell remains still the crucial topic (Keppner *et al*., 1999). For enhanced stability of the a-Si:H cell many approaches have been investigated in the past. The most promising of them are the use of hydrogen dilution (Platz *et al*., 1997; Mahan *et al*., 1991) and the hot wire deposition technique (Ziegler *et al*., 1997; Palit and Chatterjee, 1998).

RESULTS AND DISCUSSION

Hydrogenated amorphous silicon p-i-n cell: The structure chosen for the cell is p-a-SiC:H/buffer i-a-SiC:H/i-a-Si:H/n-a-Si:H. The main input parameters used for this case are given in Table 1. The absorption profiles were calculated for the standard global AM1.5 spectrum. For a 80 nm thickness of i-a-Si:H the light J-V characteristics of the cell yield a short-circuit current density of J_{sc} = 12.023 mA cm^{-2}, an open-circuit voltage V_{oc} = 0.841 volts, Fill-Factor FF = 0.690 and efficiency η = 7.638 %. These results are in coincidence with those obtained by Palit and Chatterjee (1999).

Microcrystalline silicon p-i-n cell: Hydrogenated microcrystalline silicon (μc-Si :H) is of interest for large area electronics and photovoltaics. This material exhibit a complex microstructure (crystallites, grain boundaries, amorphous phase an voids/porosity) that depends not only on the deposition methodology and parameters but also on the morphology and chemical nature of the substrate (Losurdo *et al*., 2006; Johnson *et al*., 2008).

We have simulated a microcrystalline p-i-n solar cell having the structure: p-μc-Si:H / (p/i) interface/ i-μc-Si:H/ n-a-Si:H when the mobility band gap varying according to the crystalline volume fraction. The mobility band gap of p-μc-Si:H has been assumed to be 1.6 eV at F_c ~ 18%, 1.4 eV at F_c ~ 52% and 1.2 eV at F_c ~ 70 % (Palit and Chatterjee, 1999). The crystalline volume fraction (F_c) as well as the large grain fraction in the sample were deduced from spectroscopic ellipsometry.

The principal input parameters for the doped, interconnect and absorber layers of the μc-Si:H cell are given in Table 2. For a 1300 nm thickness of i-μc-Si:H, the light J-V characteristics of the cell yields a short-circuit current density J_{sc} = 17.529 mA cm^{-2}, an open-circuit voltage V_{oc} = 0.603 volts, a Fill-Factor FF = 0.676 and an efficiency η = 7.143 %. These results are in coincidence with experimental results obtained by Johnson *et al*. (2008), Palit and Chatterjee (1998) and Nath *et al*. (2010) where the crystalline volume fraction (F_c) of the intrinsic μc-Si:H layer the gap (E_μ=1.4 eV) like that used in our simulation equal to 79% .

Tandem solar cells modelling: In this study, we have simulated two types of double junction solar cells, the first type have the following structure: p-a-SiC:H (10 nm)/buffer i-a-SiC:H(3 nm)/i-a-Si:H(80 nm) /n-a-Si:H (10 nm)/RL/p-μc-Si:H(10 nm)/(p/i) interface(3 nm)/i-μc-Si:H (1300 nm)/n-a-Si:H(10 nm) and the second type have the structure: p-a-SiC:H(10 nm)/buffer i-a-SiC:H(3 nm)/i-a-Si:H(80 nm)/n-μc-Si:H(10 nm)/RL/p-μc-Si:H(10 nm)/(p/i) interface(3 nm)/ i-μc-Si:H(1300 nm)/n-a-Si:H(10 nm).

The input parameters that simulate the output characteristics of theses stacked structures are given in Table 1 and 2. Some parameters of the doped and intrinsic microcrystalline layers have been derived from our efforts to match the measured characteristics of single and double junction cells.

The absorption profiles in the tandem cells were calculated for the standard global AM1.5 spectrum. Band

Table 1: Principal material parameters for the doped and absorber layers used to simulate the output characteristics of the a-Si: H single cell used as top cell in micromorph tandem cell

Parameters	p-a-SiC:H	I-a-SiC:H	I-a-Si:H	n-a-Si:H
L (nm)	10	3	80	10
χ (eV)	3.89	3.92	4.00	4.00
Eμ (eV)	2.00	1.96	1.86	1.80
E_{ac} (eV)	0.46	0.92	0.87	0.21
Donor doping density (cm^{-3})	0	0	0	1×10^{19}
Acceptor doping density(cm^{-3})	1.6×10^{19}	0	0	0
Effective DOS in bands (cm^{-3})	2.0×10^{20}	2.0×10^{20}	2.0×10^{20}	2.0×1020
G_{DO} ($cm^{-3}eV^{-1}$)	4.0×10^{21}	4.0×10^{21}	4.0×10^{21}	4.0×10^{21}
G_{AO} ($cm^{-3}eV^{-1}$)	4.0×10^{21}	4.0×10^{21}	4.0×10^{21}	4.0×10^{21}
E_D (eV)	0.120	0.09	0.050	0.050
E_A(eV)	0.070	0.05	0.030	0.030
μ_{e-} (cm^2/Vs)	20	20	20	20
μ_{h+} (cm^2/Vs)	4	4	4	4
$N_{D,}$NTOT (cm^{-3})	3×10^{18}	7×10^{16}	2×10^{15}	5×10^{18}
σ_n (tails) (cm^2)	10^{-17}	10^{-17}	10^{-17}	10^{-17}
σ_c (tails) (cm^2)	10^{-16}	10^{-16}	10^{-16}	10^{-15}
σ_n (midgap) (cm^2)	10^{-17}	10^{-17}	10^{-17}	10^{-17}
σ_c (midgap) (cm^2)	10^{-16}	10^{-16}	10^{-16}	10^{-15}

L: Layer thickness, χ: Electron affinity, Eμ: Mobility band gap, E_{ac} : Activation energy, E_D /E_A: Characteristic energy of the donor/acceptor-like tail states, G_{DO} /G_{AO} : Exponential prefactors of the donor/acceptor-like tail states, μ_e: Electron microscopic band mobility, μ_h: Hole microscopic band mobility, N_D: Dangling bond density of states, σ_n: Neutral capture cross sections of the defect states, σ_c: Charged capture cross sections of the defect states (Palit and Chatterjee, 1999; Poissant *et al.*, 2003).

Table 2: Principal material parameters for the doped, absorber and interconnect (RL) layers used to simulate the output characteristics of the μc-Si: H single cell used as bottom cell in micromorph tandem cell

Parameter	p-μc-Si:H	p/i interface	I-μc-Si:H	n-μc-Si:H	RL
L (nm)	10	3	1300	10	3
χ (eV)	4	4	4	4	4.3
Eμ (eV)	1.2	1.4	1.4	1.6	1.0
E_{ac}(eV)	0.06	0.64	0.64	0.03	…
Donor doping density (cm^{-3})	0	0	0	1×10^{19}	0
Acceptor doping density(cm^{-3})	3×10^{19}	0	0	0	0
Effective DOS in bands (cm^{-3})	2.0×10^{20}	2.0×10^{20}	2.0×10^{20}	2.0×10^{20}	2.0×10^{20}
G_{DO} ($cm^{-3}eV^{-1}$)	4.0×10^{21}	4.0×10^{21}	4.0×10^{21}	4.0×10^{21}	4.0×10^{21}
G_{AO} ($cm^{-3}eV^{-1}$)	4.0×10^{21}	4.0×10^{21}	4.0×10^{21}	4.0×10^{21}	4.0×10^{21}
E_D (eV)	0.02	0.05	0.02	0.05	0.07
E_A(eV)	0.01	0.03	0.01	0.03	0.04
μ_{e-} (cm^2/Vs)	100	32	32	20	30
μ_{h+} (cm^2/Vs)	25	8	8	4	6
$N_{D,}$NTOT (cm^{-3})	5×10^{16}	3×10^{17}	4×10^{16}	1×10^{17}	1×10^{20}
σ_n (tails) (cm^2)	10^{-15}	10^{-15}	1×10^{-17}	10^{-16}	10^{-14}
σ_c (tails) (cm^2)	2×10^{-14}	10^{-14}	1×10^{-15}	10^{-15}	10^{-12}
σ_n (midgap) (cm^2)	10^{-15}	10^{-15}	1×10^{-17}	10^{-16}	10^{-14}
σ_c (midgap) (cm^2)	2×10^{-14}	10^{-14}	1×10^{-15}	10^{-15}	10^{-12}

L: Layer thickness, χ: Electron affinity, Eμ: Mobility band gap, E_{ac}: Activation energy, E_D /E_A: Characteristic energy of the donor/acceptor-like tail states, G_{DO} /G_{AO}: Exponential prefactors of the donor/acceptor-like tail states; μ_e: Electron microscopic band mobility, μ_h: Hole microscopic band mobility, N_D : Dangling bond density of states, σ_n: Neutral capture cross sections of the defect states, σ_c: Charged capture cross sections of the defect states (Palit and Chatterjee, 1998; Palit *et al.*, 2000; Rubinelli *et al.*, 2001).

diagrams at thermodynamic equilibrium and under illumination at V = 0 volts of first micromorph structure: PIN(a-Si: H)/RL/PI(μc-Si: H)N(a-Si: H) and second micromorph structure: PI(a-Si: H)N(μc-Si: H)/RL/PI(μc-Si: H)N(a-Si: H) are shown in Fig.1 and 2, respectively.

We have studied the effect of varying the mobility band gap (E_μ) of the interconnect layer (RL) on solar cell efficiency. Reducing the band gap of this layer from 1.4 eV to 1.0 eV progressively increases the efficiency from 11.589 to 13.127% and V_{oc} from 1.443 to 1.541 volts, J_{sc} and FF showing a smaller change. For E_μ(RL) = 1.0 eV, the quasi-Fermi levels in the n_1 and p_2 regions on either side of the recombination layer (RL) coincide and V_{oc} attains the maximum value in the case of the second type structure (Fig. 2b2).

For both types of devices, the n_1/p_2 junction has been modelled by a highly defective RL (density of states: 10^{20} cm^{-3}) with high capture cross sections and a reduced band gap 1.0 eV (Table 2). In our modeling both the n-μc-Si:H and p-μc-Si:H layers have short tails and low activation energies (Table 2).

The substitution of the amorphous layer N_1 by another one microcrystalline in micromorph tandem cell P_1-I_1-N_1/RL/P_2-I_2-N_2 leads to an improvement of

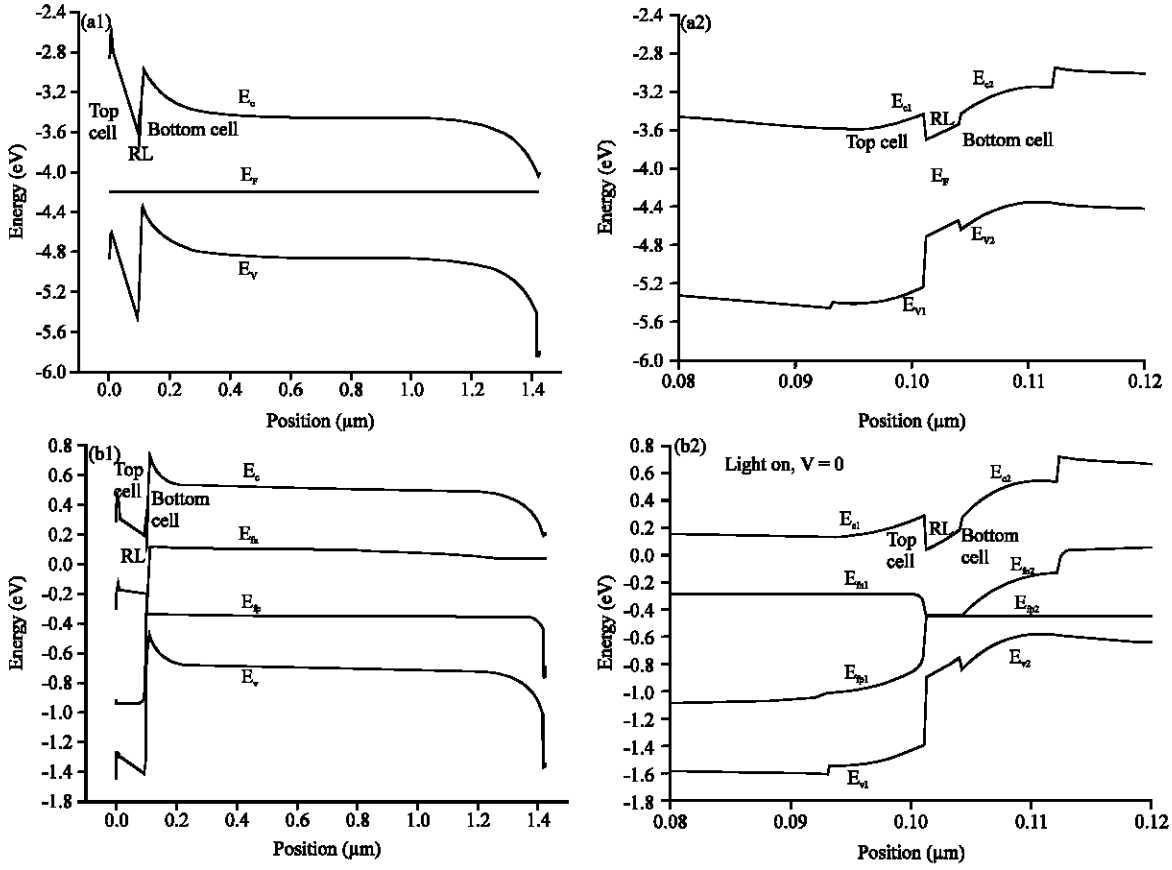

Fig. 1: Energy Band diagram of the first micromorph solar cell: p-a-SiC:H(10 nm)/buffer i-a-SiC:H(3nm) /i-a-Si:H(80nm)/ n-a-Si:H(10nm)/RL(3nm)/p-μcSi:H(10nm)/(p/i)interface(3nm)/i-μc-Si:H(1300nm)/n-a-Si:H(10nm)TheConduction band edge (E_c), the valance band edge (E_v), the electron quasi-Fermi level (E_{fn}), the hole quasi-Fermi level (E_{fp}) and the Fermi level (E_F) are indicated. (a1), (a2) Thermodynamic equilibrium (b1), (b2) Light on, V = 0

all parameters of tandem cell as indicated in Fig. 3. The modeling results shows an open-circuit voltage, V_{oc} = 1.347 V when N_1 is amorphous and V_{oc} = 1.541 V when N_1 is microcrystalline. This gain in voltage is explained as follows: first, the band discontinuity at the interface I_1/N_1 (Fig. 2b2) leads to a strong electric field (Fig. 4) because at this interface the density of state is about 10^{20} cm^{-3} eV^{-1} (so the default concentration in the gap is 2 x $10^{15}cm^{-3}$). Consequently, all the electrons diffusing from the microcrystalline layer N_1 towards the amorphous layer I_1 during the formation of the junction are trapped in the conduction band tail on a thin thickness, on the other hand, the thickness of the amorphous layer I_1 (80 nm) promotes this strong field to extend over the entire volume of the I layer as shown in Fig. 4. The presence of this strong field leads to a good collect of electron-hole pairs photogenerated from the first cell. The presence of the microcrystalline layer N_1 with a gap 1.6 eV lower than 1.8 eV (the gap of the amorphous layer N_1) followed by the reduced gap (1.0 eV) of the Recombination Layer (RL) and then the microcrystalline layer P_2 gap (1.2 eV) favor the good recombination taking place between electrons and holes photogenerated in the first and second cell, respectively. This improvement in the efficiency is supported by a best absorption in the red range and infrared spectrum by the tandem cell as shown in Fig. 5.

In tandem solar cells we have to distinguish between "good" recombination taking place between electrons and holes photogenerated in the first and second cell, respectively and "bad" recombination occurring between electrons and holes photogenerated in the same cell. Each electron-hole pair annihilated by good recombination contributes to the photocurrent. On the other hand, bad

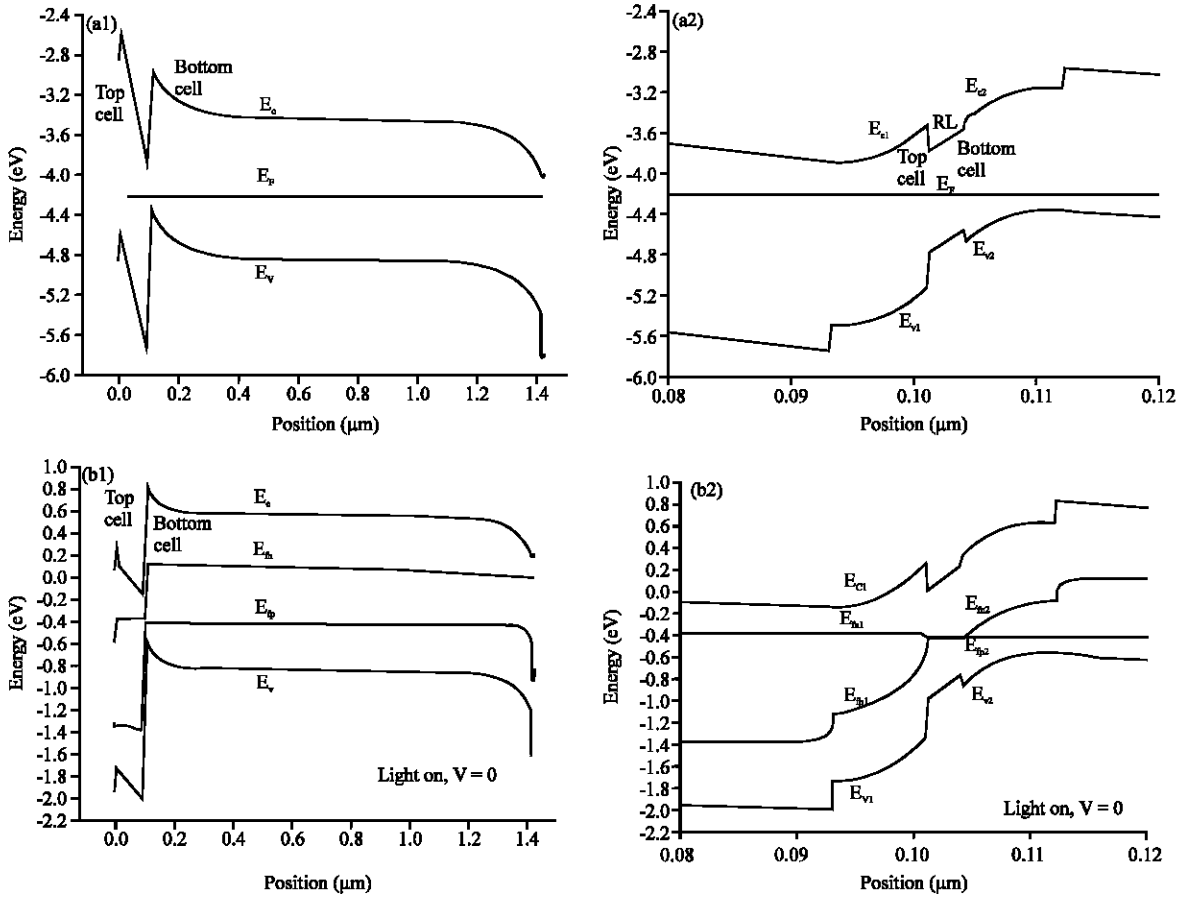

Fig. 2: Energy Band diagram of the second micromorph solar cell: p-a-SiC:H (10 nm)/ buffer I-a-SiC:H(3 nm) /I-a-Si:H (80 nm)/μc-Si:H (10 nm)/RL (3 nm)/p-μc-Si:H (10 nm)/(p/i) interface (3 nm)/i-μc-Si:H (1300 nm)/n-a-Si:H (10 nm) The Conduction band edge (E_c), the valance band edge (E_v), the electron quasi-Fermi level (E_{fn}), the hole quasi-Fermi level (E_{fp}) and the Fermi level (E_F) are indicated. (a1), (a2) Thermodynamic equilibrium (b1), (b2) Light on, V = 0

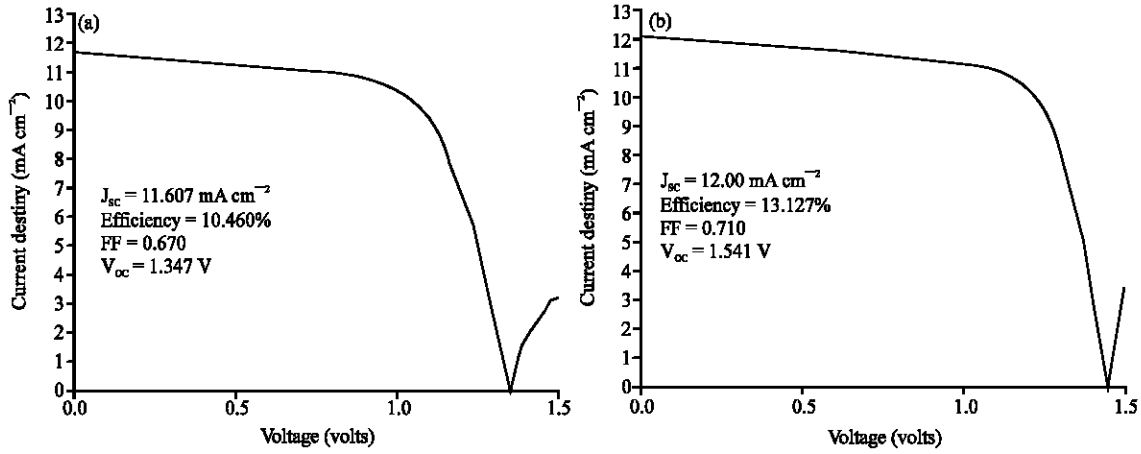

Fig. 3: Modelled illuminated J(V) characteristics of tandem solar cells: p_1-i_1- n_1(a-Si:H) /RL/ p_2- n_2 (μc-Si:H)- n_2(a-Si:H) p_1-i_1(a-Si:H)-n_1(μc-Si:H) /RL/ p_2-i_2(μc-Si:H)-n_2(a-Si:H)

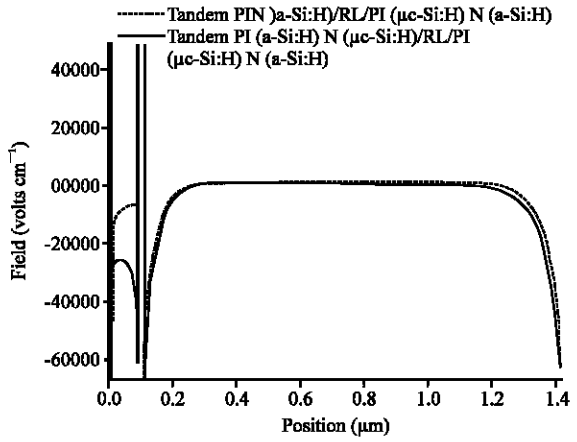

Fig. 4: Electric field profiles for tandem solar cells: p_1-i_1-n_1(a-Si:H) /RL/ p_2- n_2 (µc-Si:H)- n_2(a-Si:H) (dotted line) p_1-i_1(a-Si:H)-n_1(µc-Si:H) /RL/ p_2-i_2(µc-Si:H)-n_2(a-Si:H) (solid line)

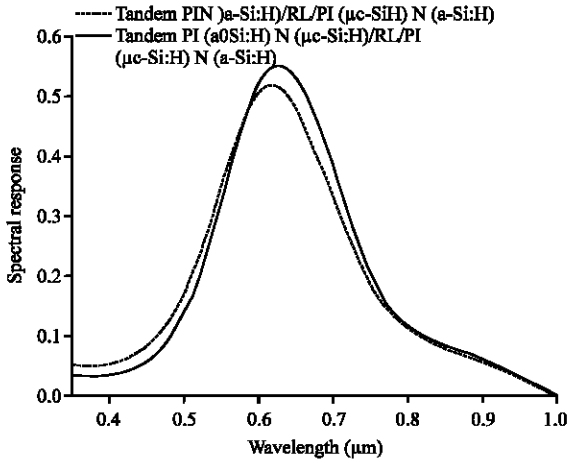

Fig. 5: Comparison of the spectral response curves of both types of double junctions solar cells: p_1-i_1-n_1(a-Si:H) /RL/ p_2- n_2 (µc-Si:H)- n_2(a-Si:H) (dotted line) p_1-i_1(a-Si:H)-n_1(µc-Si:H) /RL/ p_2-i_2(µc-Si:H)-n_2(a-Si:H) (solid line)

recombination occurring in p, i and n layers reduces the total photocurrent leading to electrical losses. Back diffusion of electrons and holes at the front and back contact, respectively, are not significant loss mechanisms in tandem cells. If the tunnel or contact junction (RL) cannot provide enough good recombination, more carriers will recombine through bad recombination and the solar cell performance will deteriorate. Other undesired effects would be the creation of a light induced dipole due to the accumulation of trapped electrons and trapped holes what would weaken the electric field in the top cell and in the bottom cell (Rubinelli *et al*., 2001) In a Tunnel-Recombination Junction (TRJ) having the simple n-µc-Si:H/RL/p-µc-Si:H structure the "good" recombination between electrons and holes photogenrated in the first and second cells, respectively, takes place in a very narrow region (~3-4 nm) located near the n/p interface and mainly inside the p-µc-Si:H layer (Rubinelli *et al*., 2001).

CONCLUSION

In this study, we have simulated a micromorph tandem cell a-Si:H/µc-Si:H using AMPS-1D.

The obtained results show clearly that the microcrystalline silicon (µc-Si:H) is a very interesting material to be used in tandem Tunnel-Recombination Junction (TRJ) because of its low mobility gap that strongly favours good recombination and its low optical absorption minimizes optical losses.

The substitution of the amorphous layer N_1 by a microcrystalline layer N_1 in micromorph tandem cell P_1-I_1-N_1/RL/P_2-I_2-N_2 leads to an improvement of the output cell parameters: J_{sc} increases from 11.607 mA cm^{-2} (for N_1 amorphous) to J_{sc}=12.00 mA cm^{-2} for (N_1 microcrystalline), FF from 0.670 to 0.710 .The V_{oc} increases from 1.347 to 1.541 V which leads to an increase of the efficiency from 10.460% for N_1 amorphous; to 13.127% when N_1 is microcrystalline. This improvement is due to the band discontinuity at the interface I_1/N_1 which leads to a strong electric field and the profiling in the energy band gap realized by N_1-P_2 microcrystalline tunnel junction between the two p-i-n subcells.

Finally the results obtained by our simulation are in good agreement with experimental results reported in the literature.

REFERENCES

Ahmed, A.H.H., E.M. Harb, M.A. Higazy and S.H. Morgan, 2008. Effect of silicon and boron foliar applications on wheat plants grown under saline soil conditions. Int. J. Agric. Res., 3: 1-26.

Al-Hadidi, M.M. and Y.K. Ibrahim, 2008. Renewable energy resources, study case for Jordan. Trends Applied Sci. Res., 3: 165-173.

Hamel, A. and A. Chibani, 2010. Characterization of texture surface for solar cells. J. Applied Sci., 10: 231-234.

Johnson, E.V., M. Nath, P. Roca i Cabarrocas, A. Abramov and P. Chatterjee, 2008. Why dose the open-circuit voltage in a micro-crystalline silicon PIN solar cell decrease with increasing crystalline volume fraction J. Non-Crystalline Solids, 354: 2455-2459.

Keppner, H., J. Meier, P. Torres, D. Fischer and A. Shah, 1999. Microcrystalline silicon and Micromorph tandem solar cells. Applied Phys. Mater. Sci. Proc., 69: 169-177.

Khatib, T.T.N., A. Mohamed, R.J. Khan and N. Amin, 2009. A novel active sun tracking controller for photovoltaic panels. J. Applied Sci., 9: 4050-4055.

Khosroshahi, R.A., N. P. Ahmadi and S. Samadzadeh, 2008. Effect of silicon on nanostructure TiAl (γ) formation kinetic via mechanical alloying method. J. Applied Sci., 8: 3727-3732.

Leblanc, F., J. Perrin and J. Schmitt, 1994. Numerical modeling of the optical properties of hydrogenated amorphous-silicon-based pin solar cells deposited on rough transparent conducting oxide substrates. J. Appl. Phys., 75: 1074-1087.

Losurdo, M., M.M. Giangregorio, A. Sacchetti, P. Capezzuto, G. Bruno, J. Càrabe, J.J. Gandia and L. Urbina, 2006. Dynamics of low temperature PECVD growth of microcrystalline silicon thin films: Impact of substrate surface teatments. J. Non-Crystalline Solids, 352: 906-910.

Mahan, H., J. Carapella, B.P. Nelson, R.S. Crandall and I. Balberg, 1991. Hot wire chemical vapor deposition: Recent progress, present state of the art and competitive opportunities. J. Applied Phys., 69: 6728-6728.

Nath, M., S. Chakraborty, E.V. Johnson, A. Abramov, P. Roca i Cabarrocas and P. Chatterjee, 2010. Performance of microcrystalline silicon single and double junction solar cells of different degrees of crystallinity. Solar Energy Mater. Solar Cells, 93: 1477-1480.

Palit, N. and P. Chatterjee, 1998. A computer analysis of double junction solar cells with a-Si:H absorber layers. Solar Energy Mater. Solar Cells, 53: 235-245.

Palit, N. and P. Chatterjee, 1999. Computer analysis of a-Si:H p-i-n solar cells with a hydrogenated microcrystalline silicon p layer. J. Appl. Phys., 86: 6879-6889.

Palit, N., A. Dasgupta, S. Ray and P. Chatterjee, 2000. Hole diffusion at the recombination junction of thin film tandem solar cells and its effect on the illuminated current-voltage characteristic. J. Applied Phys., 88: 2853-2861.

Platz, R., D. Fischer, S. Dubail and A. Shah, 1997. a-Si:H/a-Si:H stacked cell from VHF-deposition in a single chamber reactor with 9% stabilized efficiency Solar Energy Mater. Solar Cells, 46: 157-172.

Poissant, Y., P. Chatterjee and P. Roca i Cabarrocas, 2003. No benefit from microcrystalline silicon N layers in single junction amorphous silicon p-i-n solar cells. J. Applied Phys., 93: 170-174.

Rubinelli, F.A., J.K. Rath and R.E.I. Schropp, 2001. Microcrystalline n-i-p tunnel junction in a-Si:H/a-Si:H tandem cells. J. Applied Phys., 89: 4010-4018.

Shah, A., E. Vallat-Sauvain, P. Torres, J. Meier and U. Kroll *et al*., 2000. Intrinsic microcrystalline silicon(μc-Si:H) deposited by VHF-GD (very high frequency-glow discharge: A new material for photovoltaics and optoelectroncs. Mater. Sci. Eng., 69-70: 219-226.

Staebler, D.L. and C.R. Wronski, 1977. Reversible conductivity changes in discharge-produced amorphous Si. Applied Phys. Lett., 31: 292-294.

Tripathi, S. and R.O. Dusane, 2006. AMPS-1D simulation studies of electronic transport in n^+-μc-Si:H thin films. J. Non-Crystalline Solids, 352: 1105-1108.

Van den Donkera, M.N., A. Gordijna, H. Stiebiga, F. Fingera and B. Recha *et al*., 2007. Flexible amorphous and microcrystalline silicon tandem solar modules in the temporary superstrate concept. Solar Energy Mater. Solar Cells, 91: 572-580.

Veprek, S. and M.G.J. Veprek-Heijman, 1991. Open questions regarding the mechanism of plasma-induced deposition of silicon. Plasma chem. Plasma Process., 11: 323-334.

Veprek, S. and V. Marecek, 1968. The preparation of thin layers of Ge and Si by chemical hydrogen plasma transport. Solid state Elect., 11: 683-684.

Ziegler, Y., S. Dubail, C. Hof, U. Kroll and A. Shah, 1997. High efficiency p-i-n solar cells with i layer deposited by Hot-Wire Technique. Proceedings of the Conference Record of the Twenty-Sixth IEEE Photovoltaic Specialists Conference, Sep. 29-Oct. 03, Anaheim, CA, USA, pp: 687-690.